Competitive Local Laser Control of Photodissociation Reaction $HCo(CO)_4 \rightarrow HCo(CO)_3 + CO$ in Electronic Ground State

Yi Zhao and Oliver Kühn*

Institut für Chemie, Physikalische and Theoretische Chemie, Freie Universität Berlin, Takustrasse 3, D-14195 Berlin, Germany

Received: January 14, 2000; In Final Form: March 1, 2000

The performance of locally generated driving fields in the case of strong mode competition in two-dimensional models of the title reaction is investigated. The simulations are based on an all-Cartesian reaction surface Hamiltonian derived from ab initio quantum chemistry data. Here the one-dimensional reaction coordinate is defined by the Co−CO distance and motions of the $HCo(CO)_3$ fragment are described in the harmonic approximation. The influence of two substrate normal modes is investigated in detail. First, we consider the high-frequency H−Co stretching vibration, whose presence is shown to give no problem for driving the reaction coordinate. Second, we focus on a low-frequency umbrella-type mode involving the equatorial carbonyls. This mode provides a challenge to the method because of resonance and dipole gradient effects.

I. Introduction

Selective excitation and dissociation of chemical bonds by means of tailored ultrafast laser pulses is an active area of current research (for recent reviews see, for instance, refs 1 and 2). At the time being it is not the desire for controlling chemical reactions on a large scale in the laboratory that provides the driving force in this respect. Instead, the challenge is given by the problems that need to be solved along the road toward this goal. At the very heart is the proper description of the molecular system at hand. Although there has been quite some success in controlling one-dimensional model systems (in experiment and theory), real-life applications are more likely to have a multidimensional character with respect to electronic and nuclear degrees of freedom. Fortunately, chemical reactions quite often involve large-amplitude motions of a few nuclear coordinates (active coordinates) only, whereas the majority of nuclear degrees of freedom can be described within the harmonic approximation. This sets the stage for the so-called system−bath approaches to multidimensional nuclear dynamics.[3] This concept can be implemented either by defining an active coordinate along the minimum energy path[4] or along some Cartesian reaction path.[5] The two approaches essentially differ in the way the coupling between active and substrate degrees of freedom is accounted for: In the first case it is contained in the kinetic energy operator, whereas in the second case it is in the potential energy operator. In refs 6−9 it was shown that the idea of an all-Cartesian reaction surface Hamiltonian can be implemented for polyatomics on an ab initio level of quantum chemistry. Given a careful choice of the active coordinates, this allows one to simulate laser-driven nuclear dynamics in the adequate dimensionality. In particular we have studied the photodissociation reaction[8,9]

$$HCo(CO)_4 + h\nu \rightarrow HCo(CO)_3 + CO \qquad (1)$$

in the electronic ground state. The loss of the axial carbonyl group (frozen at its equilibrium geometry) has been modeled along a one-dimensional Cartesian reaction coordinate, that is, the Co−CO distance, coupled to the motions of the $HCo(CO)_3$ fragment. We note in passing that even though the alternative concept of following the minimum energy path[4] enjoys great popularity in the field of reaction dynamics (see, e.g., ref 10 and references cited therein), there has been only one application to reaction control.[11] This study, however, revealed that the complications arising from the nonadiabatic couplings necessitate further approximations.

In ref 12 a straightforward scheme for photodissociation of a bond by means of IR laser light was proposed. Here a single laser pulse of the form

$$\epsilon(t) = \epsilon_0 \sin^2(\pi t/\tau) \cos(\Omega t) \qquad (2)$$

is used to accomplish the driving of the nuclear wave packet towards dissociation. In this scheme the expectation value of the reaction coordinate resembles the behavior of a driven classical Morse oscillator. However, in contrast to the classical case, which had been studied in quite some detail already in the 1970s and 1980s,[13,14] the actual wave packet dynamics is not necessarily close to classical. For example, studying selective breaking of the H−Co bond as an alternative to eq 1 in refs 12 and 15, it was shown that for the stiff H−Co bond, wave packet dispersion is substantial, but also for the softer Co−CO bond it cannot be neglected.[8,9,12,15] The most appealing feature of this approach is the simple form of the laser pulse. Starting with the contributions of Bandrauk and co-workers,[16] chirped-pulse excitation has been favored as an efficient route to dissociation (see also ref 17). In fact, chirped-pulse vibrational ladder climbing has already been demonstrated experimentally, for example, for NO in ref 18. Chirped-pulse excitation of vibrational manifolds can also be achieved within an off-resonant Raman adiabatic passage scheme.[19,20] Alternatively to the use of chirped pulses, multipulse vibrational excitation and bond dissociation has been successfully demonstrated (see, e.g., refs 15 and 21).

Whereas the approaches mentioned so far are based on a parametrized pulse form providing enough flexibility to reach a predetermined target, optimal control theory has been developed to find those laser fields that give a maximum reaction

10.1021/jp000217f CCC: $19.00
Published on Web 05/05/2000

yield under certain physical constraints.[22] Here one defines a cost functional $J = |\langle O\rangle(T) - O_{\text{target}}(T)|^2 + J_{\text{penalty}}$, where $\langle O\rangle(T) = \langle\Psi(T)|O|\Psi(T)\rangle$ is the expectation value of some operator O taken at time $t = T$ with respect to the state vector $|\Psi(T)\rangle$. This expectation value is supposed to assume the target value $O_{\text{target}}(T)$. By solving the set of equations resulting from the condition $\delta J = 0$, with additional constraints added by the penalty term J_{penalty}, one obtains the required field $\epsilon(t)$. Via the method of Lagrangian multipliers the penalty term ensures, for example, that the field fluence is minimized and that the state vector obeys the Schrödinger equation

$$i\hbar\frac{\partial}{\partial t}|\Psi(t)\rangle = [H_0 - \mu\epsilon(t)]|\Psi(t)\rangle \tag{3}$$

Here H_0 describes the field-free evolution of the system, and the interaction with the external field $\epsilon(t)$ is considered within the semiclassical dipole approximation with the dipole operator given by μ. In practical terms the solution of the control problem has to be obtained by numerical iteration. Several efficient procedures have been suggested in this respect.[23,24] There are also comparative studies[25] showing that different numerical methods might provide different answers. This is not surprising, for the solution to the optimal control problem is not unique.

Despite these efforts, noniterative approaches might be more adequate when treating multidimensional systems. However, here the feedback for the field from the objective trajectory is accounted for only approximately, if included at all (for a discussion see ref 26). The simplest approximation, requiring the operator O to commute with the total Hamiltonian, gives the so-called local control method[26,27] (see also ref 28). Viewed as resulting from an expansion of δJ with respect to $\delta\epsilon(t)$, local control corresponds to the zero-order approximation.[26] Although this does not necessarily give the optimal field, a first-order approximation for the determination of the field has been shown to provide a significant improvement, if built on a reasonable zero-order field.[26] Local control has quite some similarities to tracking or inverse control.[29−31] The main difference between both methods is that in the tracking approach the expectation value of some observable is specified from the very beginning. By construction, tracking control provides us with a unique field for following a predefined objective. However, the price to pay is that the field may become rather unrealistic and even singularities can occur. The latter aspect and the conditions for removing such singularities have been discussed in ref 32. Local control, on the other hand, can be viewed as a sequence of optimal control steps, with the final wave function at the end point of each time step being the initial wave function for the next interval. Thus the expectation value of some objective operator is generated "on the fly".[32]

In this paper we will apply the methods of inverse and local control to study eq 1 on the basis of the Cartesian reaction surface Hamiltonian presented in ref 9. Our motivation derives from the observation that the presence of substrate normal modes renders the dissociation scheme based on the simple pulse (eq 2) inapplicable in certain cases. Besides, vibrational ladder climbing and dissociation in multidimensional systems has not yet been addressed in great detail. An early account was given by Billing and Henriksen,[33] who developed a semiclassical approach to the photofragmentation of polyatomics. More recent examples include the study of excitation of the C−C stretching vibration in planar acetylene,[34] focusing on the influence of Fermi resonances and the vibrational Stark effect. This five-dimensional treatment was made possible by exploring the idea of essential states.[35] In ref 36, bond-selective dissociation in a three-dimensional model of $HONO_2$ was investigated. The general effect of nonreactive modes on laser control in a double minimum potential has been discussed in ref 37. Control of a two-dimensional model of a hydrogen atom transfer reaction was simulated in ref 38. Here the methods of condensed-phase dynamics[3] were used to incorporate a heat bath. In fact, there are a number of studies combining the quantum master equation approach with laser control (for an account on approaches involving also excited electronic states see ref 2).[39−44]

The remaining text is organized as follows: In section II we first introduce the model Hamiltonian and then briefly review the formalism of inverse and local control. Numerical results are presented in section III and the paper is summarized in section IV.

II. Theory

A. Model System. The construction of ab initio multidimensional potential energy surfaces presents a serious challenge if more than about three degrees of freedom are involved in a reaction. In many cases, however, the reaction dynamics will not cover all the available configuration space and a partitioning into active and substrate coordinates becomes possible. Whereas the former are allowed to perform motions of arbitrary large amplitude, the latter are treated within the harmonic approximation. Here we will use the all-Cartesian formulation of this concept which had been given in ref 5 (for details of the implementation see also ref 6). Introducing (mass-weighted) normal modes $\{Q_n\}$ for the substrate coordinates and denoting the one-dimensional reaction coordinate by x, one arrives at the following (system−bath) Hamiltonian

$$H_0 = \frac{p^2}{2m} + V(x) + \frac{1}{2}\sum_j [P_j^2 + \Omega_j^2\, Q_j^2 - 2f_j(x)Q_j] \tag{4}$$

In the present case of eq 1, $V(x)$ is the one-dimensional reference potential for the motion of the reaction coordinate, which is given by the Co−CO bond length (the internal bond of the CO fragment is kept fixed at its equilibrium distance). The coupling between the reaction coordinate and the normal mode oscillators is contained in the function $f_j(x)$.

For the interaction with the external laser field we use the semiclassical Hamiltonian

$$H_F(t) = -\epsilon(t)\sum_j \mu(x, \{Q_j\}) \tag{5}$$

For the dipole moment $\mu(x, \{Q_j\})$ a low-order expansion with respect to the substrate coordinates is performed, that is,

$$\mu(x, \{Q_j\}) = \mu(x, \{Q_j = 0\}) + \sum_j \frac{\partial\mu(x,\{Q_j\})}{\partial Q_j}|_{Q_j=0} Q_j \tag{6}$$

The derivatives of the dipole moment function along the substrate normal mode coordinates can be calculated numerically, for example, by using a finite difference approximation.[9]

In ref 9 it was shown that there are two substrate normal modes that couple appreciably to the one-dimensional reaction coordinate. The potential energy and dipole moment surfaces along the reaction coordinate and the two important substrate normal modes are shown in Figure 1. Mode Q_1 can be characterized as a H−Co stretching vibration, whereas mode Q_2 is of umbrella type with respect to the equatorial carbonyls. For the following analysis it is of importance that both modes have quite different frequencies Ω_j ($\Omega_1 \approx 2000$ cm^{-1} and Ω_2

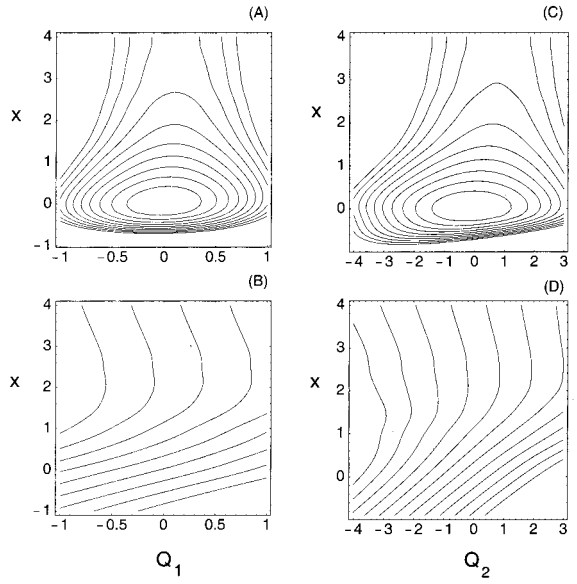

Figure 1. Potential energy surface (A, C) and dipole moment surface (B, D) for a two-dimensional model of eq 1 including a high-frequency H−Co stretching mode (A, B) and a low-frequency umbrella-type mode (C, D) (reaction coordinate in atomic units, normal mode in mass-weighted atomic units). The contour lines are plotted at: (A, C) 0.01, 0.02, ..., 0.1 hartree, (B) −3, −2.5, ... 1 Debye, (D) −4, −3.5, ... 1.5 Debye. In the numerical calculations the coordinate grid has been chosen as 128 × 256 for x and Q, respectively, with the grid boundaries given by $x = -0.94...6.00a_0$, $Q_1 = -3.0...3.0a_0$, and $Q_2 = -6.0...5.5a_0$. The gobbler function starts at $x = 4a_0$, which also defines the boundary of the interaction region in eq 13.

$\approx$ 500 cm^{-1}). Because the harmonic frequency along the reaction coordinate Ω_{sys} is about 350 cm^{-1}, unwanted resonance effects can be expected when driving the reaction coordinate with a spectrally broad laser pulse. This effect will be of particular importance because of the dipole gradient, which points basically along the umbrella-type normal mode in the vicinity of the equilibrium geometry [cf. Figure 1 panel (D)].

The quite different characteristics of the two normal modes allows us to study their influence on the dynamics of the reaction coordinate separately in section III.

B. Laser Control. One of the main results of ref 9 was the observation that the inclusion of the umbrella-type mode renders the dissociation control with a simple laser pulse of the form of eq 2 impossible because of resonance and dipole effects. An appreciable part of the available laser energy is consumed for heating the substrate normal mode. This is not the case for the high-frequency H−Co mode; because of the large frequency mismatch the presence of this mode is no problem for the laser-driven dissociation with the pulse (eq 2).

To take up the challenge provided by the very competitive umbrella-type mode we will apply the methods of tracking and local control in the following.[29−31] Tracking or inverse control is based on an intuitive guess for an optimal trajectory O_{track}. The Heisenberg equations of motion for the quantum mechanical expectation value of the operator O associated to O_{track} are then inverted to give the field necessary for following this track. Because the calculation of the expectation value requires knowledge about the state vector, the equation for the field is coupled to the Schrödinger (eq 3) (for a detailed discussion see ref 29). If the considered operator commutes with the field-dependent part of the Hamiltonian, that is, with the dipole operator, one encounters a so-called trivial singularity in the field, which can be removed by stepping to the higher-order derivatives of O.[32] To be specific, let us consider the case of position tracking, that is, O corresponds to the reaction coordinate operator x. Because $[x, \mu(x)] = 0$ we have to use the equation of motion for the respective momentum p, which is given by

$$\frac{\mathrm{d}}{\mathrm{d}t}\langle p\rangle = \frac{1}{i\hbar}\langle [p, H_0]\rangle - \frac{1}{i\hbar}\langle [p, \mu\epsilon(t)]\rangle = \frac{\mathrm{d}}{\mathrm{d}t}p_{\mathrm{track}} \tag{7}$$

In the second line we made use of the condition that the evolution of the momentum expectation value should follow the predefined track p_{track}. Equation 7 is easily inverted to give the field as

$$\epsilon(t) = \frac{m\frac{\mathrm{d}}{\mathrm{d}t}p_{\mathrm{track}} + \left\langle\frac{\mathrm{d}V}{\mathrm{d}x}\right\rangle}{\left\langle\frac{\mathrm{d}\mu}{\mathrm{d}x}\right\rangle} \tag{8}$$

We note that this expression does not include any restriction on the field as far as it concerns its fluence. In practice the use of this method therefore requires a careful choice for the tracking variable p_{track}. This holds in particular if the concept is extended to more dimensions as proposed in ref 29.

An alternative is provided by local competitive tracking suggested in ref 31. Here the desired track is not specified a priori but determined from the instantaneous expectation values entering the right-hand side of the equations of motion for the momentum. To drive the reaction coordinate toward dissociation it is reasonable to assume that the objective trajectory is specified by

$$\frac{\mathrm{d}}{\mathrm{d}t}p_{\mathrm{track}} = -\left\langle\frac{\mathrm{d}V(x)}{\mathrm{d}x}\right\rangle + \gamma_x\frac{\mathrm{d}}{\mathrm{d}t}\langle p\rangle \tag{9}$$

where γ_x is a constant playing the role of a damping parameter. Equating eq 9 with eq 7 one obtains the field as $\epsilon(t) = \gamma_x\langle p\rangle/\langle \mathrm{d}\mu/\mathrm{d}x\rangle$. As shown in ref 31, this expression does not perform well in practical calculations, particularly in situations where the wave packet is rather delocalized. Instead it has been suggested[31] to formulate a related variational problem on the basis of the cost functional

$$J = \left\langle\left[\gamma_x p - \epsilon(t)\frac{\mathrm{d}\mu}{\mathrm{d}x}\right]^2\right\rangle \tag{10}$$

Minimizing this functional gives the field as

$$\epsilon(t) = \frac{\gamma_x}{\sqrt{E_x(t)}}\frac{\mathrm{Re}\left\langle\frac{\mathrm{d}\mu}{\mathrm{d}x}p\right\rangle}{\left\langle\left(\frac{\mathrm{d}\mu}{\mathrm{d}x}\right)^2\right\rangle} \tag{11}$$

As has been pointed out in ref 31, the fact that the field is proportional to the momentum ensures very efficient energy deposition into the reaction coordinate. Note that we have included a factor $1/\sqrt{E_x(t)}$ where $E_x(t)$ is the expectation value of the system energy. This factor prevents an exponential increase of the momentum and thus of the energy.[31] As we will show below, this factor also leads to fields of more moderate strengths. Equations 10 and 11 are easily extended to the multidimensional case. One obtains the locally optimized field as

$$\epsilon(t) = \frac{W_x(t)\frac{\gamma_x}{\sqrt{E_x(t)}}\mathrm{Re}\left\langle\frac{\partial}{\partial x}\mu(x,\{Q_n\})p\right\rangle + \sum_j W_j(t)\frac{\gamma_j}{\sqrt{E_j(t)}}\mathrm{Re}\left\langle\frac{\partial}{\partial Q_j}\mu(x,\{Q_n\})P_j\right\rangle}{W_x(t)\left\langle\left[\frac{\partial}{\partial x}\mu(x,\{Q_n\})\right]^2\right\rangle + \sum_j W_j(t)\left\langle\left[\frac{\partial}{\partial Q_j}\mu(x,\{Q_n\})\right]^2\right\rangle} \quad (12)$$

Here we introduced damping parameters for the different degrees of freedom as γ_x and γ_j.[31] This will allow us to trigger the motion along one coordinate while damping competing degrees of freedom (see below). The relative weight of this desired motion of the different coordinates is specified by the functions $W_x(t)$ and $W_j(t)$. Note that in ref 31 these weights have been taken as constants. However, for one of the applications presented below it was essential to allow for a time dependence at this point (cf. section III). Finally, we included the factors $1/\sqrt{E_x(t)}$ and $1/\sqrt{E_j(t)}$, with $E_x(t)$ and $E_j(t)$ being the instantaneous expectation value of the energy for the different (uncoupled) degrees of freedom (see above).

In the following we will present results for the different methods using the dissociation probability

$$P_{\mathrm{diss}}(t) = 1 - \int_{V_{\mathrm{int}}} \mathrm{d}x\, \mathrm{d}Q |\Psi(x,Q;t)|^2 \quad (13)$$

as a measure for successful driving. In eq 13 V_{int} denotes that part of the potential energy surface where the gradient along the exit channel is appreciably different from zero.

III. Results

A. One-Dimensional Case. To provide a reference case, we first study the laser-driven dynamics along the one-dimensional reaction coordinate only. Throughout we will use the fast Fourier transform method, together with a symmetrically split time evolution operator for propagation of the wave functions on a grid (grid parameters in caption of Figure 1).[45,46] To prevent reflection from the grid boundaries along the reaction coordinate we used a sin-type gobbler function.[47]

We start with the position tracking according to eqs 7 and 8. The objective trajectory is given by an antidamped classical motion in the potential $V(x)$ (see middle panel of Figure 2, dashed line). Tracking this trajectory presents no problem at all, as can be seen in the middle panel of Figure 2. The dissociation yield is close to 100 % (see inset) at the expense of a very strong field, which is shown in the upper panel of Figure 2. In the initial part of the dynamics the field is very similar to the simple analytical form (2). This is in accord with the fact that the pulse (eq 2) drives the Morse-type oscillator in a way that the behavior of $\langle x \rangle(t)$ basically corresponds to that of a classical antidamped oscillator. Whereas the driving via the field of eq 2 gives appreciable dissociation even after the wave packet becomes delocalized,[8] in the present case the field strength strongly increases when the variance of the coordinate expectation value increases, as shown in Figure 2. This implies that it is very demanding for the field to ensure that the system follows a classical trajectory.

Next we consider the same problem using local control theory. Here the field is given by eq 11. Neglecting for the moment the factor $1/\sqrt{E_x(t)}$, we find the dynamics shown in Figure 3. Obviously, the local control approach is better suited to deal with situations where the wave packet becomes delocalized. The maximum field strength is a factor of two lower than in the position tracking case, without deterioration of the reaction yield.

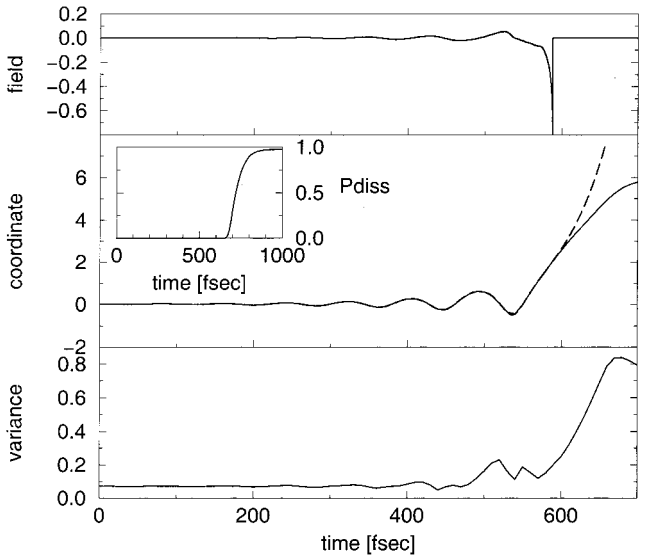

Figure 2. Position tracking control of one-dimensional reaction coordinate. The objective trajectory $x_{\mathrm{track}}(t)$ is generated from the antidamped classical equation of motion $\mathrm{d}^2x/\mathrm{d}t^2 = -\mathrm{d}V(x)/\mathrm{d}x + \gamma \mathrm{d}x/\mathrm{d}t$ with $\gamma = 20$. Field, position, and variance of the position are given in atomic units.

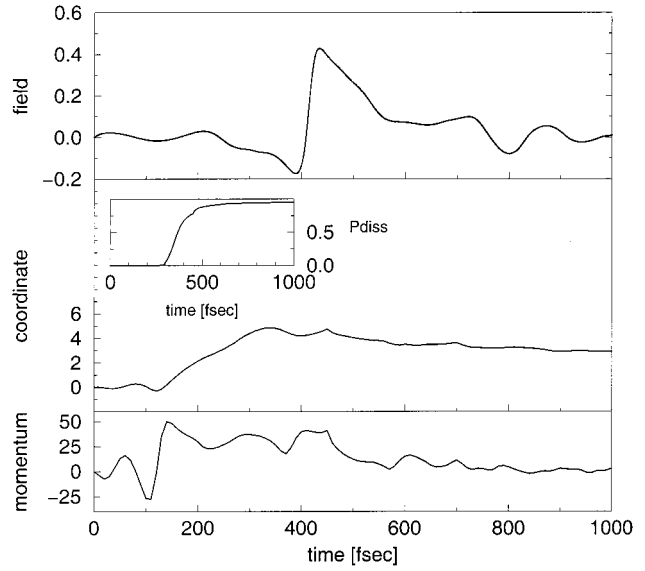

Figure 3. Local control of the one-dimensional motion along the reaction coordinate according to eq 11 without using the energy prefactor. For a choice of $\gamma_x = 0.0307$ the wave packet remains quite localized (not shown) while moving into the exit channel. Field, position, and momentum are given in atomic units.

Comparing the field (upper panel) and the expectation value of the momentum operator (lower panel) shows that the dipole gradient plays an important role for the determination of the field (cf. eq 11), that is, the field does not follow directly the momentum of the system.

Including the energy denominator in eq 11 reduces the maximum field strength by a factor of 10. The results of the numerical simulation are plotted in Figure 4. The dissociation yield is about 65% and, in contradistinction to Figure 3, the coordinate expectation value more closely resembles the dynamics of the classical antidamped Morse-type oscillator. The power spectrum of the field is shown in the inset of the upper panel in Figure 4. It is dominated by a peak at 330 cm^{-1}, a frequency that is close to the $0 \rightarrow 1$ vibrational transition frequency along the reaction coordinate ($\Omega_{\mathrm{sys}} \approx 350\ \mathrm{cm}^{-1}$). Thus the mechanism

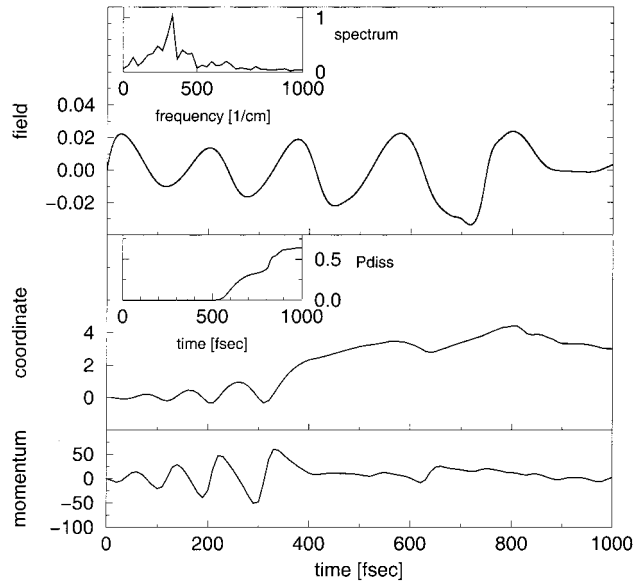

Figure 4. Same as in Figure 3 but including the energy prefactor in eq 11. Field, position, and momentum are given in atomic units.

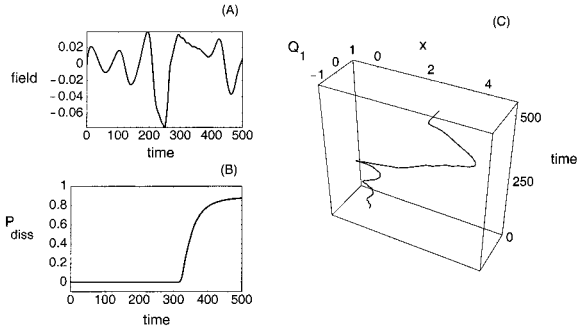

Figure 5. Local control in for the two-dimensional including the reaction coordinate and the high-frequency mode [cf. Figure 1 (A) and (B)]. The energy prefactor in eq 12 has not been taken into account. (A) Laser field, (B) dissociation probability, (C) trajectory (field and coordinates in atomic units, time in femtoseconds). The weight functions in eq 12 are taken to be constant, $W_x = 0.8$ and $W_1 = 0.2$. The damping parameters are $\gamma_x = 0.45$ and $\gamma_1 = -1.0$.

of local driving can be considered as being similar to the case of the simple field of eq 2 that was studied in refs 8 and 9.

B. High-Frequency Q_1 Mode. As a first example for a substrate mode that presents a competition to the laser driving of the reaction coordinate, we consider the high-frequency H−Co stretching mode. In Figure 5 we show the expectation value of the coordinates together with the driving field and the time-dependent dissociation probability. The time-dependent energy factors in eq 12 have been omitted because reaction control could be achieved using moderate field strength already in this case. Further, it was not necessary to use time-dependent weight functions in eq 12, and we have taken $W_x = 0.8$ and $W_1 = 0.2$ for simplicity.

The power spectrum of the driving field has a major peak at 280 cm^{-1}, that is, close to the frequency reaction coordinate Ω_{sys}. Because the normal mode frequency Ω_1 is much higher, this mode is basically not excited during dissociation. This can be seen from the coordinate expectation values in Figure 5 but also from the snapshots of the wave packet dynamics shown in Figure 6. From Figure 6 we further see that the moving wave packet remains compact up to the dissociation. The overall behavior is in accord with the results of the simulations that used the simple pulse form eq 2.[9]

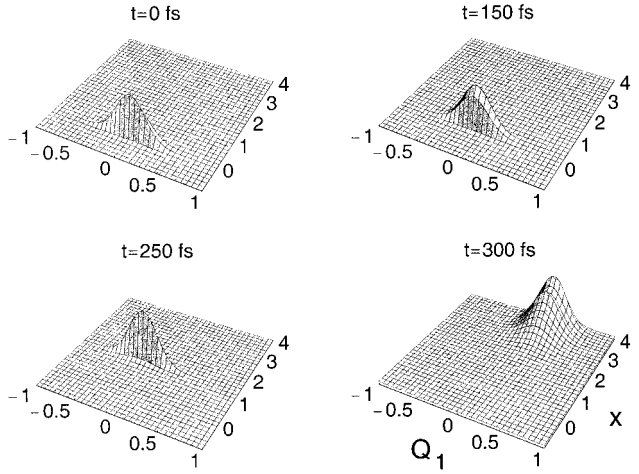

Figure 6. Snapshots of the wave packet dynamics corresponding to the situation in Figure 5 (absolute values scaled for visualization).

C. Low-Frequency Q_2 Mode. Next we focus on the influence of the umbrella-type substrate normal mode. Because a simple pulse of the form in eq 2 failed to trigger dissociation in this case, we expect the two-dimensional (x,Q_2) system to provide a more stringent test for the local control approach.

For the weighting functions we used (cf. also ref 29)

$$W_x(t) = \cos^2(\alpha t) \tag{14}$$

and

$$W_2(t) = \sin^2(\alpha t) \tag{15}$$

It turned out that the resulting dynamics are very sensitive to the actual value chosen for the parameter α. The general dependence is in accord with the idea of a stroboscopic weighting provided by eqs 14 and 15. If α is of the order of the $0 \rightarrow 1$ transition frequency along the reaction coordinate, dissociation could be achieved with a certain flexibility in the damping parameters γ_x and γ_2. For a much larger $\alpha > \Omega_{sys}$, no control was possible. On the other hand, for $\alpha < \Omega_{sys}$ we observed dissociation, but with a yield that was very sensitive to the choice of the damping parameters. No control on a time scale of about 1 ps was possible for constant weight functions.

First we present the results for the case where the energy denominator in eq 12 had been neglected. The results of the numerical simulation are summarized in Figures 7 and 8. Inspecting Figure 7, we first notice that the dissociation yield is close to 100%. When contrasting this success with the zero yield obtained for the simple-pulse driving case, one has to consider that the driving field has a rather exotic shape and it becomes very strong as well [cf. panel (A) in Figure 7]. Thus it is very likely that the Born−Oppenheimer approximation breaks down, and processes like ionization would have to be considered in a more realistic model (cf. ref 48). Because this is beyond the scope of the present investigations, we will view the results shown in Figure 7 as a reference case that provides useful information about the mechanism leading to the dissociation within the adopted model. In panel (C) of Figure 7 we have plotted the time-dependent coordinate expectation values. Apparently, the initial part of the dynamics can be characterized as leading mostly to an excitation of the substrate normal mode. In view of the dipole surface shown in Figure 1(D), this does not come as a surprise. However, with increasing energy the moving wave packet covers a region where the potential coupling $f_2(x)$ becomes important as well. The

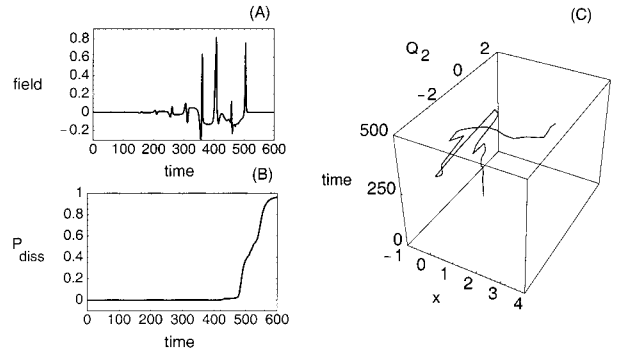

Figure 7. Local control in for the two-dimensional including the reaction coordinate and the low-frequency mode [cf. Figure 1 (C) and (D)]. The energy prefactor in eq 12 has not been taken into account. (A) Laser field, (B) dissociation probability, (C) trajectory (field and coordinates in atomic units, time in femtoseconds). The weight functions are chosen according to eqs 14 and 15 with a stroboscopic frequency of $\alpha = 330$ cm^{-1}. The damping parameters are $\gamma_x = 0.85$, $\gamma_2 = -35.0$.

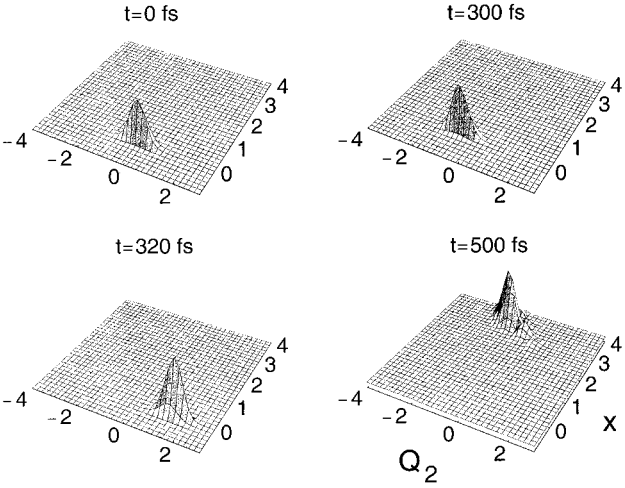

Figure 8. Snapshots of the wave packet dynamics corresponding to the situation in Figure 7 (absolute values scaled for visualization).

concerted action of both driving and coupling finally guides the wave packet into the exit channel. Looking at the wave packet snapshots in Figure 8, the most striking observation is that there is only little delocalization. In other words, the motion is to a good approximation that of a classical particle. On the basis of our experience with the one-dimensional limit, we expect that upon inclusion of the energy factors in eq 12, the field will behave more moderately also in this two-dimensional case. In fact, the numerical results shown in Figure 9 support this supposition. The maximum field strength is reduced by a factor of eight and the overall behavior of $\epsilon(t)$ is much smoother than in Figure 7. However, this behavior comes along with a lower dissociation yield of about 12%. As a consequence of the reduced antidamping of the reaction coordinate dynamics $[\propto \gamma_x/\sqrt{E_x(t)}]$, it takes a much longer time to deposit enough energy into this coordinate such that dissociation occurs. The respective dynamics of the coordinate expectation values covers large parts of the bound-state potential energy surface. This behavior, however, can no longer be interpreted in terms of classical dynamics. In fact, the snapshots of the wave packet plotted in Figure 10 reveal that already after 500 fs, that is, well before any dissociation takes place, the wave packet is covering most of the available configuration space. The circumstance that despite this almost complete delocalization there is appreciable dissociation setting in at about 1.5 ps points to the strength of the competitive local control method.

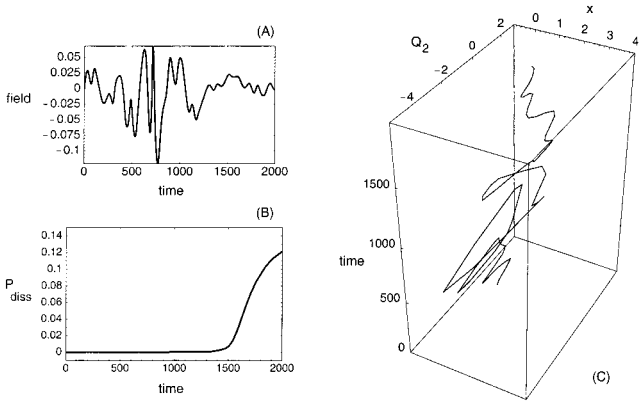

Figure 9. Local control in according to eq 12 for the two-dimensional including the reaction coordinate and the low-frequency mode [cf. Figure 1 (C) and (D)]. (A) Laser field, (B) dissociation probability, (C) trajectory (field and coordinates in atomic units, time in femtoseconds). The weight functions are chosen according to eqs 14 and 15 with a stroboscopic frequency of $\alpha = 220$ cm^{-1}. The damping parameters are $\gamma_x = 0.09$, $\gamma_2 = -3.0$.

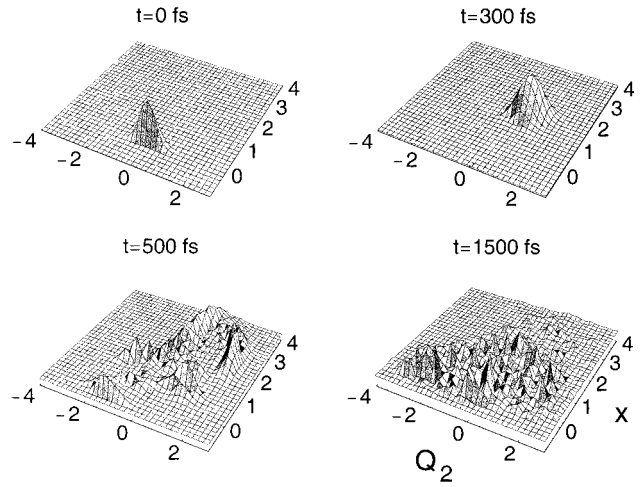

Figure 10. Snapshots of the wave packet dynamics corresponding to the situation in Figure 9 (absolute values scaled for visualization).

IV. Summary

Local competitive control of two-dimensional models of the ground-state photodissociation reaction (eq 1) has been studied on the basis of an ab initio all-Cartesian reaction surface Hamiltonian. After the failure of the approach to drive the reaction with the simple pulse (eq 2) in the presence of the low-frequency umbrella-type substrate normal mode reported in refs 8 and 9, our initial intention was to use optimal control theory.[26] This iterative procedure, however, turned out to be numerically very demanding because of the present need for a large grid. The noniterative local control approach, on the other hand, performed well in producing reasonable reaction yields for moderate laser pulse shapes. To accomplish this goal, the use of a stroboscopic-type weight function for the different objectives, that is, antidamping of the reaction coordinate and damping of the substrate normal mode, proved to be crucial in the case of strong mode competition. Further, it was shown that the inclusion of a time-dependent energy factor that gives an additional damping[31] led to a considerable smoothening of the pulse shape and a reduction of the maximum pulse strength needed for efficient dissociation. Finally, we found the dynamics upon inclusion of the high-frequency normal mode to be rather classical, that is, the dissociation proceeds without substantial wave packet dispersion. On the other hand, in the presence of

the low-frequency mode and for a reasonable pulse form, the wave packet becomes delocalized over the available configuration space already well before dissociation. However, even in this case, the local control method is able to guide a good fraction of the wave packet toward dissociation.

Acknowledgment. We gratefully acknowledge stimulating discussions with Prof. J. Manz (Berlin) and Prof. Y.-J. Yan (Hong Kong). This work has been supported by the Deutsche Forschungs-gemeinschaft (Sfb450) and the Deutscher Akademischer Austauschdienst.

References and Notes

(1) Manz, J. In *Femtochemistry and Femtobiology: Ultrafast Reaction Dynamics at Atomic-Scale Resolution*; Sundström, V., Ed.; London: Imperial College Press, 1997, p 80.
(2) Rice, S. A. *Adv. Chem. Phys.* **1997**, *101*, 213.
(3) May, V.; Kühn, O. *Charge and Energy Transfer Dynamics in Molecular Systems*; Berlin: Wiley-VCH, 2000.
(4) Miller, W. H.; Handy, N. C.; Adams, J. E. *J. Chem. Phys* **1980**, *72*, 99.
(5) Ruf, B. A.; Miller, W. H. *J. Chem. Soc., Faraday Trans. 2* **1988**, *84*, 1523.
(6) Orel, A. E.; Kühn, O. *Chem. Phys. Lett.* **1999**, *304*, 285.
(7) Naundorf, H.; Organero, J. A.; Douhal, A.; Kühn, O. *J. Chem. Phys.* **1999**, *110*, 11286.
(8) Naundorf, H.; Orel, A. E.; Zhao, Y.; Kühn, O. *Faraday Discuss.* **1999**, *113*.
(9) Orel, A. E.; Zhao, Y.; Kühn, O. *J. Chem. Phys.* **2000**, *112*, 94.
(10) Nguyen, K. A.; Jackels, C. F.; Truhlar, D. G. *J. Chem. Phys* **1995**, *102*, 3188.
(11) Shah, S. P.; Rice, S. A. *Faraday Discuss.* **1999**, *113*, 319.
(12) Zhao, Y.; Kühn, O. *Chem. Phys. Lett.* **1999**, *302*, 7.
(13) Walker, R. B.; Preston, R. K. *J. Chem. Phys.* **1977**, *67*, 2017.
(14) Goggin, M. E.; Milonni, P. W. *Phys. Rev. A* **1988**, *37*, 796.
(15) Kühn, O.; Manz, J.; Zhao, Y. *Phys. Chem. Chem. Phys.* **1999**, *1*, 3103.
(16) Chelkowski, S.; Bandrauk, A. D.; Corkum, P. B. *Phys. Rev. Lett.* **1990**, *65*, 2355.
(17) Chelkowski, S.; Bandrauk, A. D. *J. Chem. Phys.* **1993**, *99*, 4279.
(18) Maas, D. J.; Duncan, D. I.; Vrijen, R. B.; van der Zande, W. J.; Noordam, L. D. *Chem. Phys. Lett.* **1998**, *290*, 75.
(19) Chelkowski, S.; Gibson, G. N. *Phys. Rev. A* **1995**, *52*, R3417.
(20) Davis, J. C.; Warren, W. S. *J. Chem. Phys.* **199**, *110*, 4229.
(21) Paramonov, G. K. In *Femtosecond Chemistry*; Manz, J., Wöste, L., Eds.; Weinheim: Verlag Chemie, 1995; Vol. 2, p 671.
(22) Peirce, A.; Dahleh, M.; Rabitz, H. *Phys. Rev. A* **1988**, *37*, 4950.
(23) Zhu, W.; Botina, J.; Rabitz, H. *J. Chem. Phys.* **1998**, *108*, 1953.
(24) Zhu, W.; Rabitz, H. *J. Chem. Phys.* **1998**, *109*, 385.
(25) Sola, I. R.; Santamaria, J.; Tannor, D. J. *J. Phys. Chem. A* **1998**, *102*, 4301.
(26) Zhu, W.; Rabitz, H. *J. Chem. Phys.* **1999**, *110*, 7142.
(27) Ohtsuki, Y.; Kono, H.; Fujimura, Y. *J. Chem. Phys.* **1998**, *109*, 9318.
(28) Kosloff, R.; Rice, S. A.; Gaspard, P.; Tersigni, S.; Tannor, D. J. *Chem. Phys.* **1989**, *139*, 201.
(29) Gross, P.; Singh, H.; Rabitz, H.; Mease, K.; Huang, G. M. *Phys. Rev. A* **1993**, *47*, 4593.
(30) Lu, Z.-M.; Rabitz, H. *J. Phys. Chem.* **1995**, *99*, 13731.
(31) Chen, Y.; Gross, P.; Ramakrishna, V.; Rabitz, H. *J. Chem. Phys.* **1995**, *102*, 8001.
(32) Zhu, W.; Rabitz, H. *J. Chem. Phys.* **1999**, *110*, 1905.
(33) Billing, G. D.; Henriksen, N. E. *Chem. Phys.* **1988**, *119*, 205.
(34) Liu, L.; Muckerman, J. T. *J. Chem. Phys.* **1999**, *110*, 2446.
(35) Kaluza, M.; Muckerman, J. T. *Chem. Phys. Lett.* **1995**, *239*, 161.
(36) Oppel, M.; Paramonov, G. K. *Chem. Phys.* **1999**, *250*, 131.
(37) Karmacharya, R.; Gross, P.; Schwarz, S. D. *J. Chem. Phys.* **1999**, *111*, 6864.
(38) Došlić, N.; Sundermann, K.; González, L.; Mó, O.; Giraud-Girard, J.; Kühn, O. *Phys. Chem. Chem. Phys.* **1999**, 1, 1249.
(39) Sugawara, M.; Fujimura, Y. *J. Chem. Phys.* **1994**, *101*, 6586.
(40) Kühn, O.; Malzahn, D.; May, V. *Int. J. Quantum Chem.* **1996**, *57*, 343.
(41) Korolkov, M. V.; Paramonov, G. K.; Schmidt, B. *J. Chem. Phys.* **1996**, *105*, 1862.
(42) Korolkov, M. V.; Manz, J.; Paramonov, G. K. *J. Phys. Chem.* **1996**, *101*, 13927.
(43) Ohtsuki, Y.; Zhu, W.; Rabitz, H. *J. Chem. Phys.* **1999**, *110*, 9825.
(44) Yuan, J. M.; Liu, W.-K.; Hayashi, M. T.; Lin, S. H. *J. Chem. Phys.* **1999**, *110*, 3823.
(45) Kosloff, D.; Kosloff, R. *J. Comp. Phys.* **1982**, *52*, 35.
(46) Leforestier, C.; Bisseling, R.; Cerjan, C.; Feit, M. D.; Friesner, R. *J. Comp. Phys.* **1991**, *94*, 59.
(47) Child, M. S. *Mol. Phys.* **1991**, *72*, 89.
(48) Bandrauk, A. D.; Aubanel, E. E.; Gauthier, J. M. In *Molecules in Laser Fields*; Bandrauk, A. D., Ed.; New York: Marcel Dekker, 1994; p 109.